X-RAY MICROTOMOGRAPHY AND DIC TECHNIQUE TO ANALYSE THE HYGROEXPANSION OF PLANT-BASED FIBROUS MATS FOR COMPOSITES MATERIALS

J. Viguié[1], P.J.J. Dumont[2*], S. Rolland du Roscoat[1], P. Vroman[3], L. Orgéas[1], B. Vermeulen[4]. J.-F. Bloch[2]

[1]*Laboratoire Sols-Solides-Structures-Risques (3S-R), CNRS / Université de Grenoble, BP 53, 38041Grenoble cedex 9, France*
[2]*Laboratoire de Génie des Procédés Papetiers (LGP2), CNRS / Grenoble INP, BP 65, 38402 Saint-Martin-d'Hères cedex, France*
**pierre.dumont@grenoble-inp.fr*

Keywords: Flax fibre mat, X-ray tomography, Hygroexpansion, Digital Image Correlation

Abstract
This study aims at describing the microstructural deformation phenomena of flax fibre mats induced by changes in the relative humidity (RH) of the ambient air. At the macroscopic scale, the in-plane variations of the mats' dimensions were studied using a specially developed device. At the microscopic scale, in situ synchrotron X-ray microtomography 3D images were used to characterise 3D evolution of their microstructure using both image analysis procedures and a Digital Image Correlation (DIC) technique to measure the porous and fibrous phase evolutions as well as the displacement field within such materials. Hysteresis phenomena for the absorption and desorption properties, as well as for the hygroexpansion of the fibrous mats are observed. Results also emphasise the influence of the anisotropic structure of the tested fibrous mats. At the microscopic scale, the analysis of the X-ray microtomography images highlights the combined evolution of the porosity and of the geometry of the fibrous phase during the RH cycles.

1 Introduction

The reduction of the ecological impact of structural materials has become an important issue. In this context, natural fibres are considered as a credible alternative to synthetic fibres being used as reinforcement in polymer composites. Apart from being extracted from renewable resources, natural fibres have also interesting mechanical properties which can make them compete with glass fibres [1]. However, their spreading in the composite domain is limited by the high variability of their microstructure and physical and anisotropic mechanical properties, their poor adhesion with organic thermoplastic matrices, or their high sensibility to water absorption and the resulting poor dimensional stability. Many studies are devoted to overcome some of these drawbacks. Pre-treatments of natural fibres are investigated [2]. Other ways may consist of adapting current composite processing routes to natural fibres or developing new routes. This implies that the hygroexpansive behaviour of natural fibres (or network made up of natural fibres) is well understood and controlled. Therefore, this study aims at describing the deformation phenomena of plant-based fibre mats that are induced by changes in the relative humidity (RH) of the ambient air at the macroscopic scale as well as at the mesoscopic scale of the fibre network. Macroscopic hygroexpansion is investigated using

devices that were initially developed for paper hygroexpansion analysis. Deformation phenomena at the microscopic scale are studied using X-ray microtomography coupled with Digital Image Correlation (DIC) technique. Materials and processing conditions are first exposed. Then the characterization method of the microstructure by X-ray microtomography is described as well as hygroexpansion measurement techniques. Results at the macroscopic scale are detailed and the observed microstructural evolution with the relative humidity change is described.

Figure 1. Schematic description of the production process of the needled flax fibre mats.

2 Materials and processing conditions

Tested non-woven fibrous mats were formed with a mixture of 90 % in weight of slender bundles of flax fibres (mean length 45 mm, mean diameter 25 μm) and 10 % in weight of slender polypropylene fibres (mean diameter 15 μm). They were produced by successive opening, carding, cross lapping operations to form webs of required basis weight. These webs were consolidated by needle punching, and finally hydro-linking operations to obtain the required consolidation for the as-processed fibrous mats. The whole process is described in Fig. 1. Note those operations confer preferential operations to the fibrous reinforcement. The cross lapping results in particular in an in-plane preferential orientation of fibres along the mat cross direction. The obtained mat has a basis weight of 250 g/m2 and a thickness about 1 mm.

3 Microstructure characterization by X-ray microtomography

Microtomographic 3D images were acquired at the European Synchrotron Radiation Facility (ESRF) in Grenoble, France. During data acquisition, a parallel and monochromatic X-ray beam irradiates the sample. Radiographs of the X-ray beam (20.5 keV) passing through the sample are recorded for different angular positions (1500) between 0° and 180°. According to the typical size of the fibrous constituents of the fibrous mat, a voxel size of

$2.5 \times 2.5 \times 2.5\ \mu m^3$ was chosen, giving an imaged volume of $3750 \times 3750 \times 1125\ \mu m^3$. A filtered back-projection algorithm is applied to reconstruct the 3D structure of the sample using the scanned radiographs. When performing absorption-based X-ray microtomography, the reconstructed 3D volume represents a 3D map of the coefficient of x-ray absorption of the sample constituents. The values of the absorption coefficients are represented as different values of grey level coded in 32 bits. In order to obtain quantitative descriptors of the sample structure, image treatment operations were performed. These operations consist of segmenting the image to respectively distinguish the porous and fibrous phases. This was performed using segmentation algorithms developed by Rolland du Roscoat *et al.* [3] for the analysis of paper imaged by X-ray microtomography. The obtained segmented volume is depicted in Fig. 2.

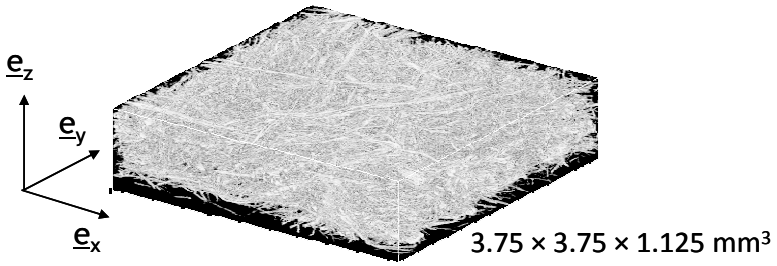

Figure 2. Segmented volume of the flax fibre mat imaged by X-ray microtomography.

The porosity of the binarised volumes can be evaluated as the ratio of the voxels belonging to the pore phase, to the whole number of voxels in the volume. The specific surface area, defined as the ratio of the total interstitial surface area to the bulk volume, can be linked to the number of crossings (or intercepts) of a line with the pore-fibre interfaces by unit length (this measure is also called the mean intercept number) in all the space directions [3].
The relative humidity of the air surrounding the sample was in situ controlled during the image acquisition using a wet air generator. The sample was first stabilized at 50%. RH. Then, four relative humidity steps were performed: 50%→20%→50%→80%→50% RH. The duration (10 min) of each relative humidity step was chosen so as to reach an equilibrium configuration of the sample. The macroscopic hygroexpansive strain ε_{zz} in the thickness of the sample was calculated as the ratio of the sample thickness measured at the end of each relative humidity step to the sample thickness measured at the end of the first relative humidity stabilisation step.

4 Moisture sorption and hygroexpansion measurements

4.1 Moisture and hygroexpansion setups

The moisture content evolution of the fibrous mat was measured at 23 °C with the especially designed Varimass® device (Techpap, Grenoble, France) for sixteen relative humidity steps: 50%→35%→20%→35%→50%→65%→80%→65%→50%→35%→20%→35%→50%→65%→80%→65%→50% RH. This cycle was repeated 25 times. Each step lasted 5000 s. Hygroexpansive strains associated to the same relative humidity steps were recorded with the Varidim® device (Techpap, Grenoble, France). These systems include a wet air generator, with a compressed air pre-treatment device and a control unit, a test chamber where the samples are placed, and a computer and two software applications that allow the entire process to be controlled. The air generator provides the test chamber with conditioned air. In the Varimass® system, the mass of a sample m_s is recorded using a precision balance (±0.5 mg). Then, the moisture content c is calculated using the mass of the dry sample m_{sdry} (oven dried for 24 h at 105°C) as follows:

$$c = \frac{m_s - m_{sdry}}{m_{sdry}} . \quad (1)$$

The Varidim® system allows the length variation of ten samples of 15 mm in width and 150 mm in length to be measured. The samples are vertically fastened with magnetic clamps at both extremities, whereas the bottom clamp can slide and is attached to a LVDT displacement sensor. The accuracy of the measurement reaches ±3 μm. The in-plane hygroexpansive strain ε_h is expressed as follows:

$$\varepsilon_h = \frac{\Delta L}{L_0}, \quad (2)$$

where L_0 is the length at the end of the first relative humidity step at 50% RH, and ΔL is the length variation. Tested samples were cut along the machine direction (θ=0°), along the cross direction (θ=90°) and along the direction θ=45°.
It was observed that the moisture content and the hygroexpansive strain of the tested fibrous mats tended both to stabilize at the end of each relative humidity step.

4.2 Digital image correlation technique
In order to study the hygroexpansive behaviour of the fibre mat, a 2D Digital Image Correlation (DIC) technique was used. This technique relies on comparing the pattern matching of two grey intensity images coded in 32 bits obtained before and after a relative humidity change. This comparison allows the measurement of the relative displacement of the points of the two images. These images were extracted from the 3D microtomographic volume. Indeed, such images of the sample exhibit a random grey intensity distribution, which can be used as a random speckle pattern. The correlation was led between one cross section parallel to the plane ($\underline{\mathbf{e}}_x$, $\underline{\mathbf{e}}_z$) extracted in the middle part of the reconstructed volume at 50% RH and images of the corresponding cross section extracted from the volume scanned at 20% and 80% RH. The whole procedure to find the corresponding cross section as well as to perform the correlation using the 7D® software is described in detail in Viguié *et al.* [4].

5 Experimental macroscopic results

Fig. 3(a) depicts the evolution of the axial hygroexpansive strain ε_h in the machine direction (MD, θ=0°) with respect to the moisture content c. The axial hygroexpansive strain shows a slight hysteresis which can be quantified by measuring the maximum of the moisture content variation between sorption and desorption at the same hygroexpansive strain. This parameter is noted ΔC_{max}. This hygroexpansive strain is defined as the median axial strain and is noted ε_{median}. The variation between the value of the hygroexpansive strain at the lowest moisture content and the value reached at the highest moisture content is noted $\Delta\varepsilon$. Figs. 3(b) and 3(c) exhibit the evolution of $\Delta\varepsilon$ and ε_{median} respectively with respect to the number of relative humidity cycles. It appears that the amplitude of the hygroexpansive strain is rather limited in the in-plane machine direction (reaching 0.11%) and tends to remain nearly constant with the number of humidity cycles. However the median strain exhibits a significant increase from the first cycle (lower than 0.01%) to the 25th cycle (0.05%) which may result from a creep phenomenon.

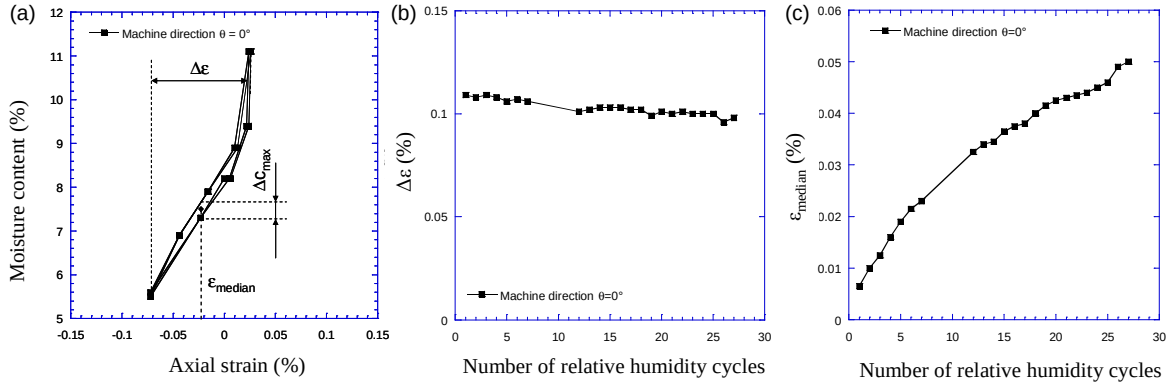

Figure 3. (a) Evolution of the axial hygroexpansive strain ε_h in the machine direction with respect to the moisture content. (b) Evolution of the amplitude of the axial hygroexpansive strain $\Delta\varepsilon$ in the machine direction and (c) evolution of the median axial strain ε_{median} with respect to the number of relative humidity cycles.

Fig. 4(a) exposes the evolutions of the axial hygroexpansive strain in the machine direction (θ=0°), in the cross direction (θ=90°) and in the intermediate direction (θ=45°) with respect to the moisture content c. A strong influence of the fibrous mat anisotropy is revealed. In order to better study this dependence, Figs. 4(b) and 4(c) show respectively the evolutions of ΔC_{max} and $\Delta\varepsilon$ with respect to the orientation θ. It can be noticed that the hysteresis effect is 1.5 to 2 times higher in the intermediate direction than in the machine and cross directions. Furthermore the amplitude of the axial hygroexpansive strain doubles between the machine direction and the cross direction, reaching 0.22% in the cross direction.

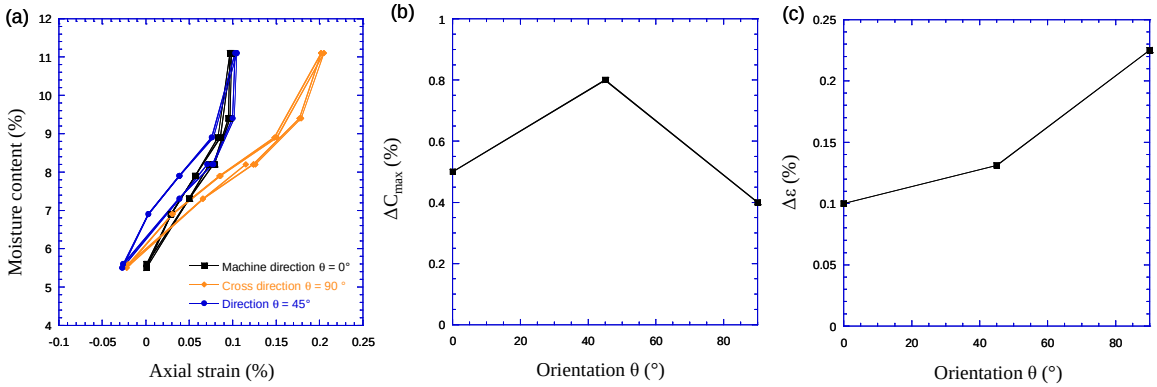

Figure 4. (a) Evolution of the axial hygroexpansive strain ε_h in the machine direction, in the cross direction and in the direction defined by θ=45° with respect to the moisture content c. (b) Evolution of the maximum of the moisture content variation ΔC_{max} at the same hygroexpansive strain, and (c) evolution of the amplitude of the axial hygroexpansive strain $\Delta\varepsilon$ with respect to the orientation θ.

Fig. 5 presents the evolution of the out-of-plane hygroexpansive strain ε_{zz} estimated directly from the sample thickness variations using the microtomographic 3D images or by DIC during the relative humidity cycle 50%→20%→50%→80%→50% RH. The in-plane hygroexpansive strains ε_{xx}, in the machine direction and ε_{yy}, in the cross direction, are also plotted in order to be compared with the out-of-plane values. The evolutions of ε_{zz} measured directly using 3D images and of ε_{zz} measured by DIC show the same trend. Nonetheless, a slight difference is observed in values which are reached. This can be attributed to the top and bottom layers at the mat/air interface which are not taken into account when performing the DIC measurement. It is worth noting that the hygroexpansive strain is very low when the relative humidity of the ambient air varies between 50% and 20% RH and sharply increases between 20% and 80% RH. When the relative humidity goes back to 50% RH, a significant irreversible hygroexpansive strain is recorded (between 5 and 7%). Such behaviour may be

related to large changes in the microstructure of the small sample of the fibre mat induced by such large amplitude relative humidity cycle. Besides, at 80% RH, the hygroexpansive out-of-plane strain is 30 to 50 times higher than in-plane attesting for important anisotropic hygroexpansive behaviour of the flax fibre mat.

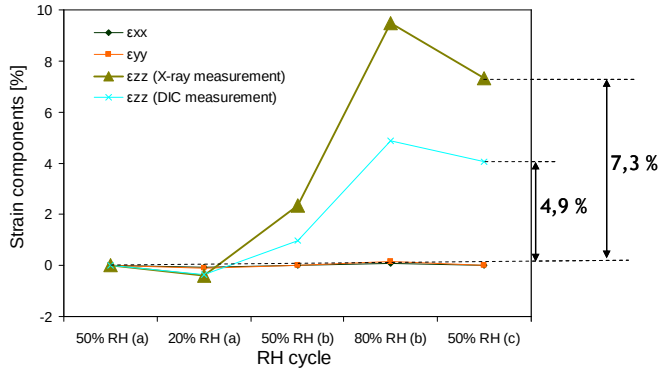

Figure 5. Evolution of the out-of-plane hygroexpansive strain ε_{zz} measured directly or by DIC using the X-ray microtomography images, and evolutions of the in-plane hygroexpansive strains in the machine direction noted ε_{xx} and in the cross direction noted ε_{yy} extracted from the previous macroscopic results, for the relative humidity cycle 50%→20%→50%→80%→50% RH.

6 Microstructural evolution during hygroexpansion

Fig. 6(a) depicts the variation of the porosity during the relative humidity cycle 50%→20%→50%→80%→50% RH measured using segmented microtomographic 3D images (*cf.* §3). The porosity first significantly increases (by 1.8%) when the relative humidity of the surrounding air varies from 50% to 20% and then decreases when the relative humidity increases up to 80% RH. At such relative humidity value, it is 0.8% higher than at the reference state (50% RH). Finally the porosity reaches its higher value at the final relative humidity of 50% RH. This evolution can be correlated with the variation of the mean intercept length L_z measured respectively for the pore and fibre phases in the out-of-plane direction, and revealed in Fig. 6(c). From 50% to 20% RH, L_z within the fibre phase decreases by 2.8%, showing the shrinkage of the thickness of the fibrous phase. However, such shrinkage is compensated by an increase of the mean intercept length within the porous phase having the same order of magnitude. As a consequence, the total variation of the fibre mat thickness is close to zero as revealed in Fig. 6(d) which depicts the variation of the total thickness during the whole investigated relative humidity cycle.

When the relative humidity varies from 20% to 80% RH, L_z in the fibre phase increases to be finally slightly higher than the value measured at the reference state (50% RH). For the same humidity steps, L_z in the pore phase does not show a significant evolution and remains around 3% higher than in the reference state value. This phenomenon well explains the porosity decrease exhibited in Fig. 6(a) at 80% RH, and the significant increase of the thickness of the fibre mat (around 5%), as revealed in Fig. 6(d). At the last relative humidity step of 50 % RH, L_z in the fibre phase is significantly reduced to be 2% lower than in the reference state. Simultaneously, the mean intercept length increases in the pore phase. This behaviour can be corroborated with the observed relatively weak decrease of the total thickness of the fibre mat when the relative humidity passes from 80% to 50% RH (3% higher than the reference state value), see figure 6d.

Fig. 6(b) depicts the variation of the specific surface area during the humidity cycle. This parameter tends to follow the evolution of L_z of the fibre phase. The specific surface reaches its lower value at 20% RH (-2%) and its higher value at 80% RH (+2.5%). As a conclusion, the microstructure is significantly influenced by the variation of the relative humidity of the

surrounding air: the microstructure tends to be irreversibly opened during the humidity variations.

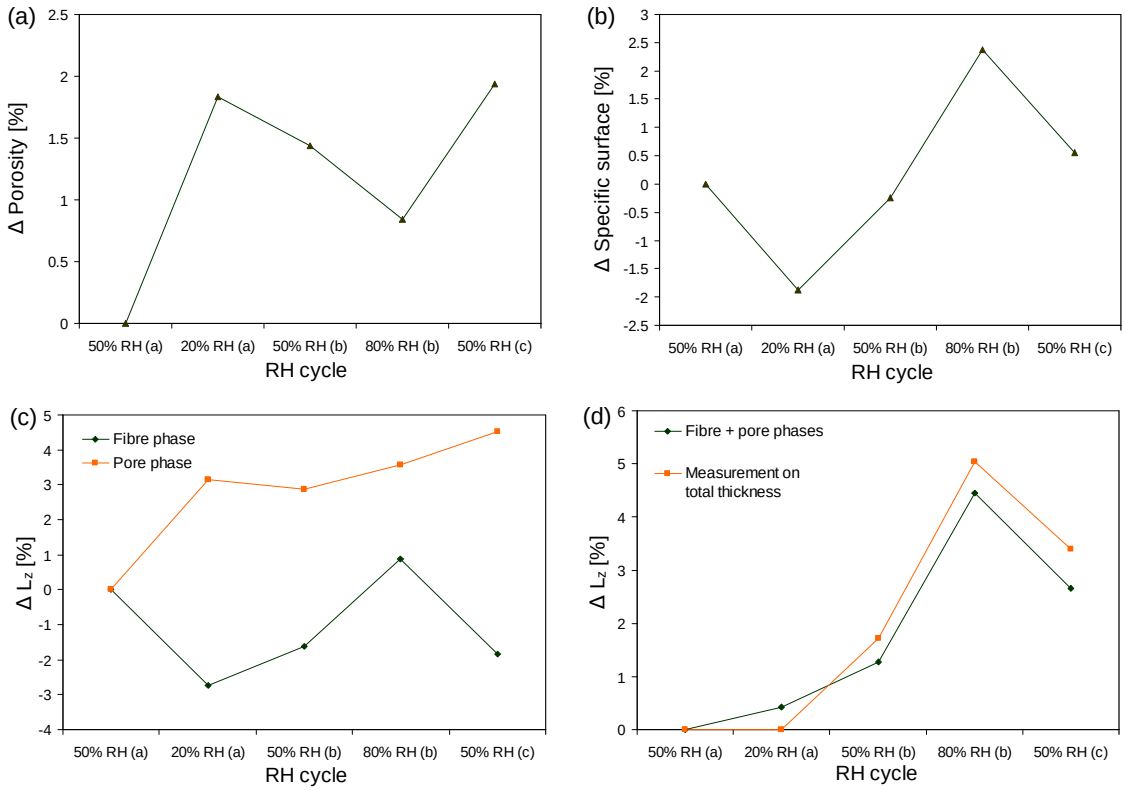

Figure 6. (a) Variation of the porosity, (b) variation of the specific surface, (c) variation of the mean intercept number in the $\underline{\mathbf{e}}_z$ direction of the pore and fibre phases, (d) variation of the mean intercept number in the $\underline{\mathbf{e}}_z$ direction of the sum of pore and fibre phases compared with the variation of the total thickness of the fibre mat through the relative humidity cycle 50→20→50→80→50 % RH.

In order to study more accurately the evolution of the structure at the scale of the fibre network (mesoscopic scale), the DIC method was applied to the microtomographic images as it has been previously described (§4). The procedure was performed for three parallel cross sections of the studied sample. Similar results could be obtained whatever the studied cross sections. Thus, in the following, results of a representative cross section are presented. Fig. 7 shows maps of the out-of-plane strain component ε_{zz} related to a relative humidity change from 20% to 50% RH, Fig. 7(a), and a relative humidity change from 50% to 80% RH, see Fig. 7(c). Maps show that ε_{zz} is largely heterogeneous. This reveals a complex deformation phenomenon at the scale of the fibre network. Nevertheless it appears that ε_{zz} significantly varies through the thickness of the sample but remains rather homogeneous at a given z coordinate. In order to analyse precisely this phenomenon, the average strain $\langle\varepsilon_{zz}\rangle$ profiles calculated through the thickness are plotted in Figs. 7(b) and 7(d), respectively for the two relative humidity steps. These profiles depict a large heterogeneity in the thickness direction. We can well distinguish three parts of the fibre mat thickness which behave differently. For the humidity step from 50% to 20% RH, the upper part of the fibrous mat (300 µm in thickness) is slightly compressed (around 0.35%), the medium part (around 200 µm in thickness) is less deformed and the lower part tends to be more compressed (around 0.5%). For the humidity step from 50% to 80% RH, the same upper region significantly expands (around 6%), the medium region is less deformed reaching a minimum expansion around 4% and finally the lower part expands around 5%. As a conclusion, it appears that the fibre mat does not behave in the same manner throughout its thickness; the middle region tends to be

less deformed during the relative humidity change. An analysis of the evolution of the fibre content through the thickness may bring some insights to better understand this behaviour [4].

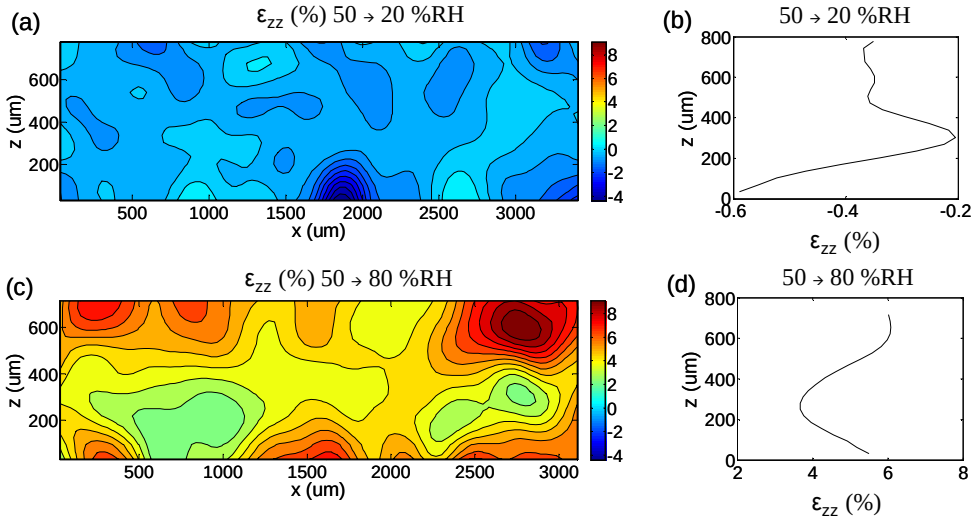

Figure 7. (a) Map of the hygroexpansive strain in thickness ε_{zz} in the plane ($\underline{\mathbf{e}}_x$,$\underline{\mathbf{e}}_z$) and (b) profile in the thickness direction of the average value of the hygroexpansive strain described in (a) for the relative humidity step 50%→20% RH. (c) Map of the hygroexpansive strain in thickness ε_{zz} in the plane ($\underline{\mathbf{e}}_x$,$\underline{\mathbf{e}}_z$) and (b) profile in the thickness direction of the average value of the hygroexpansive strain described in (c) for the relative humidity step 50%→80% RH.

7 Conclusion

The hygroexpansive behaviour of flax fibre mats used as composite reinforcement materials was studied both at the mesoscopic and microscopic scales, using in this latter case 3D images obtained by X-ray microtomography. The acquired experimental data allow a better understanding of the hygroexpansive mechanisms of such materials, which exhibit hysteresis and a great anisotropy, and which result in an irreversible and heterogeneous opening of the material's microstructure as revealed by the analysis of the simultaneous evolution of the porous and fibrous phases throughout the material's thickness. Such original data will be relevant to provide improved hygroexpansive models for plant fibre-based reinforcement materials, and to improve the understanding of their behaviour during storage and processing situations.

References

[1] Bodros E., Pillin I., Montrelay N., Baley C. Could biopolymers reinforced by randomly scattered flax fibres be used in structural applications? *Composites Science and Technology*, **67**, pp. 462-470 (2007).

[2] Susheel K., Kaith B.S., Inderjeet K. Pretreatments of natural fibers and their application as reinforcing material in polymer composites - A review. *Polymer Engineering and Science*, **49**, pp. 1253-1272 (2009).

[3] Rolland du Roscoat S., Decain M., Thibault X., Geindreau C., Bloch J.-F. Estimation of microstructural properties from synchrotron X-ray microtomography and determination of the REV in paper materials. *Acta Materialia*, **55**, pp. 2841-2850 (2007).

[4] Viguié J., Dumont P.J.J., Mauret E., Rolland du Roscoat S., Vacher P., Desloges I., Bloch J.-F. Analysis of folding board hygroexpansive behaviour by correlation of images obtained by X-ray microtomography. *Journal of Materials Science*, **46**, pp. 4756-4769 (2011).